Unifying Kondo coherence and antiferromagnetic ordering in the honeycomb lattice

Saeed Saremi, Patrick A. Lee, and T. Senthil

Phys. Rev. B **83**, 125120 — Published 29 March 2011

DOI: 10.1103/PhysRevB.83.125120

Unifying Kondo coherence and antiferromagnetic ordering in the honeycomb lattice

Saeed Saremi, Patrick A. Lee, and T. Senthil
Department of Physics, Massachusetts Institute of Technology,
77 Massachusetts Avenue, Cambridge, MA 02139

In this paper, we describe a mechanism by which the destruction of the Kondo coherence at the same time gives rise to antiferromagnetic ordering. This picture is in contrast to the Doniach picture of the competition of Kondo coherence and antiferromagentic orderring. Our study is done in the honeycomb lattice at half-filling, where Kondo coherence gives rise to a Kondo insulator. We go beyond mean-field (large N) formulation of Kondo coherence in Kondo lattices and consider excitations we call Kondo vortices. A Kondo vortex is a configuration where at its core the Kondo amplitude vanishes while far away from the core it retains the uniform Kondo amplitude. A Kondo vortex in our model brings 4 zero modes to the chemical potential. The zero modes play a crucial role as they allow us to construct spin-1 operators. We further study the transformation of these spin-1 Kondo vortex operators under various symmetry transformations of the Kondo Hamiltonian, and find a class of operators that transform like an antiferromagnetic order parameter. This gives a novel picture of how one can create antiferromagnetic ordering by proliferating Kondo vortices inside a Kondo coherent phase. We finish by studying the universality class of this Kondo vortex mediated antiferromagnetic transition, and conclude that it is in the $O(3)$ universality class.

I. INTRODUCTION

Understanding the evolution between the non-magnetic Fermi liquid and the antiferromagnetic metal in heavy fermion materials is one of the major challenges in the field of strongly correlated electrons[1,2]. Much attention has focused on the possibility of a direct second order quantum critical point (QCP) separating these two phases[3–5]. In some cases there is good evidence[1,2,7] – from the studies of the evolution of the Fermi surface – pointing to the *simultaneous* collapse of Kondo screening and anti-ferromagnetic (AF) scales at the QCP. Such a direct second order phase transition is rather hard to understand theoretically. Instead one might have expected an intermediate phase with coexistence (see Fig. 1) of both Kondo screening and magnetic order or novel intermediate phases with neither Kondo screening nor magnetic order[9] (see Fig. 2). These more natural possibilities are in fact realized in some cases[10–12]. But the apparent direct second order transition between the heavy Fermi liquid and magnetic metal seen in some cases remains a mystery, and may well play a key role in understanding of the observed strong non-Fermi liquid physics in the quantum critical region above the QCP (see Fig. 3).

The conventional approach in formulating the competition between Kondo screening and magnetic ordering is to construct a mean-field theory by introducing Kondo coherence and anti-ferromagnetic order parameters. This framework (from the the well-known work of Doniach[8]) leads to the phase diagram of Fig. 1, where the AF transition happens inside the Kondo screening phase. The theory of quantum critical modes at this antiferromagnetic QCP is known as the Hertz-Millis theory.[13] The Hertz-Millis theory (in the light of new experiments) fails on two fronts. First, it fails[14] to explain the strong non-Fermi liquid behavior (i.e. *linear* temperature resistivity) above the AF critical point seen in the wide variety of experiments.[2] More importantly, the Hertz-Millis picture is in direct contradiction with the new experiments where the *sudden* change in Fermi surface topology at the critical point is observed.[6,7] This is because a nonzero Kondo hybridization at the AF quantum critical point guarantees a *continuous* change in Fermi surface across the QCP. To incorporate the sudden change in Fermi surface topology one is forced to consider the scenario depicted in Fig. 3.

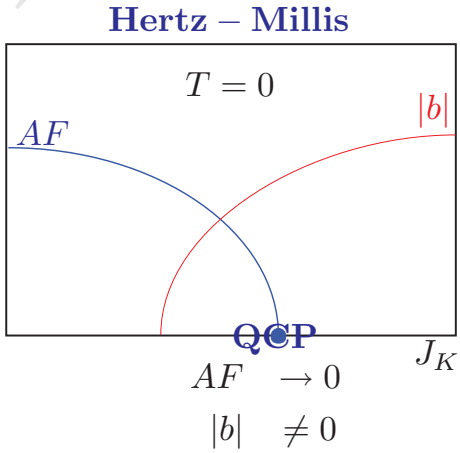

FIG. 1: Hertz-Millis picture of AF quantum critical point in heavy fermions: The AF transition happens inside the Kondo phase. b characterizing the Kondo coherence is defined in the next section.

Despite the proposal of Fig. 3, we do not have a theoretical understanding of why Kondo and AF phases should collapse at a single point. The root of the problem is that, in present theories, destruction of the Kondo coherence has nothing to do with emergence of AF ordering. They are just two completely different phases which are competing with each other and in this framework an overlap is unavoidable. We need to find a way to "unify" these two distinct phases. By unification of

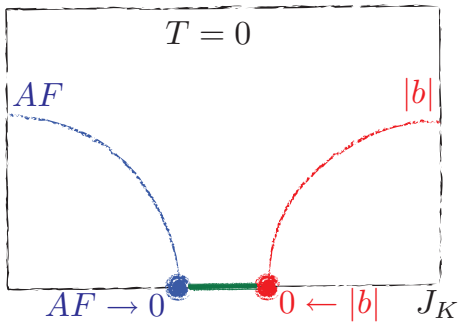

FIG. 2: In this scenario AF and Kondo transitions are separate giving rise to an exotic metal phase in the intermediate region. One possibility is local moments form spin liquid while c-electrons form small Fermi surface.[9]

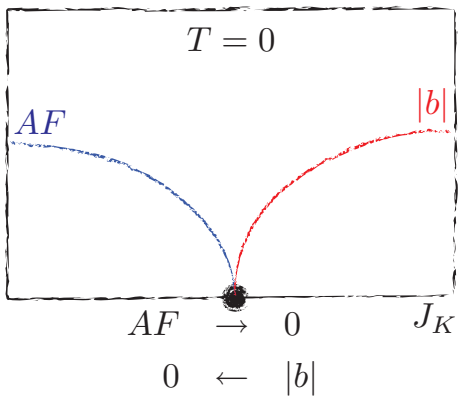

FIG. 3: Simultaneous collapse of AF and Kondo scales: A new paradigm for AF transition consistent with the sudden jump in Fermi surface topology at the QCP. There are no established theories that explain why this *simultaneous* collapse should happen. We need to find a way to *unify* these two distinct phases.

Kondo and AF phases we mean finding a mechanism in which the destruction of Kondo coherence at the same time gives birth to AF ordering, or vice versa. The yet to be developed unification picture will complement the competition picture of Doniach. But the unified theory is the theory that would matter to understand the QCP *itself*.

In Ref. 16 we took a step in this direction by studying excitations we called Kondo vortices inside the Kondo coherence phase. Kondo vortex (KV) is a configuration where at its core the Kondo *amplitude* vanishes while far away from the core it retains the uniform mean-field value. In the model we have studied we have shown that we can localize a spin-1 at the vortex core. Now we can imagine destroying the Kondo phase by proliferating Kondo vortices while at the same time giving birth to a magnetic ordering.

This approach in destroying the Kondo phase by proliferating Kondo vortices is quite novel, and to make progress we have focused on a very specific model, i.e. the honeycomb lattice at half-filling. What is special (but not necessarily exclusive) to this model is that in the presence of a KV 4 *zero modes* are brought to the chemical potential. The presence of zero modes allows us to construct spin-1 vortex creation operators, since we have the *freedom* to occupy the zero modes. In the absence of zero modes we are forced to occupy the Dirac sea with up and down spins and the resulting state would be a magnetically featureless spin singlet state. After studying the transformation of the spin-1 vortex operators under various lattice symmetries, we find a class of these KV operators that transform like an AF order. This gives a plausible scenario of how one might be able to unify the Kondo phase and AF phase, since we can destroy the Kondo phase (by proliferating Kondo vortices) and at the same time create AF ordering.

We chose half-filled honeycomb lattice for two reasons. First, the particle-hole symmetry guarantees that the chemical potential remains at zero for any Kondo and gauge field configurations. The other is that the Dirac spectrum near the (isolated) Dirac nodes enables us to study the Kondo vortex in the continuum limit. However, the disadvantage of this model is that the Kondo phase is not realized as a heavy fermi liquid phase, but as a Kondo *insulator*. Furthermore since the honeycomb lattice is a *bipartite* lattice the AF phase is also an insulator. Therefore we do not have a Fermi surface in neither of those phases, and we can not address the evolution of the fermi surface (a central issue of the heavy fermion QCP) in our model.

Here is the outline of the paper. In Sec. II we describe the Kondo insulator phase, and construct the KV configuration in the Kondo insulator phase. In Sec. III we focus on the spectrum of the Kondo Hamiltonian in the presence of a KV, and in particular we discuss the zero modes the KV generate. In Sec. IV we construct spin-1 vortex operators using the zero modes we have found, and in Sec. V we study how these spin-1 vortex operators transform under various symmetries of the Kondo-Heisenberg Hamiltonian. Having this transformation table, we find a class of these operators that transform like an AF order. In Sec. VI we discuss the universality class of the AF transition mediated by proliferation of Kondo vortices, and show that (in our model) it is an $O(3)$ transition. We conclude by highlighting the main results of this paper.

II. KONDO VORTICES IN THE KONDO INSULATOR

Our starting point is the Kondo-Heisenberg Hamiltonian given by

$$\hat{H} = -t \sum_{\langle ij\rangle\alpha} \left(c^\dagger_{i\alpha} c_{j\alpha} + H.c. \right) + J_K \sum_i \boldsymbol{s}_i \cdot \boldsymbol{S}_i + J_H \sum_{\langle ij\rangle} \boldsymbol{S}_i \cdot \boldsymbol{S}_j, \tag{1}$$

where $c^\dagger_{i\alpha}$ is the conduction electron creation operator at site i with spin flavor $\alpha \in \{\uparrow, \downarrow\}$, $\boldsymbol{S}_i$ is the localized spin and

$$\boldsymbol{s}_i = \frac{1}{2} c^\dagger_{i\alpha} \boldsymbol{\sigma}_{\alpha\beta} c_{i\beta} \tag{2}$$

is the conduction electron spin operator.

Let us identify the Hibert space of the localized spins at site i by $\{|\Uparrow\rangle_i, |\Downarrow\rangle_i\}$ and the one for the conduction electrons by $\{|\uparrow\rangle_i, |\downarrow\rangle_i\}$. In the large J_K limit the ground state $|GS\rangle$ (at half-filling) is given by the direct product of the singlets $|0\rangle_i = \frac{1}{\sqrt{2}} \left(|\Uparrow\rangle_i |\downarrow\rangle_i - |\Downarrow\rangle_i |\uparrow\rangle_i\right)$ at each site:

$$|GS\rangle = \bigotimes_i |0\rangle_i \,. \tag{3}$$

Since all conduction electrons are bound to localized spins through the singlet formation, we end up with an insulator ground state, known as the Kondo insulator. It is worth noting that the ground state above is the strong Kondo coupling ground state. However the ground state remains an insulator as one decreases J_K. To have a mean-field picture of the Kondo coherence – and therefore the Kondo insulator – we write localized spin $\boldsymbol{S}_i$ at site i using slave fermions f_i:

$$\boldsymbol{S}_i = \frac{1}{2} f^\dagger_{i\alpha} \boldsymbol{\sigma}_{\alpha\beta} f_{i\beta}. \tag{4}$$

They are called *slave* fermions since to match the *localized* spin Hilbert space, the Hilbert space of the f fermions must be *constrained*:

$$\sum_\alpha f^\dagger_{i\alpha} f_{i\alpha} = 1. \tag{5}$$

This constrained is enforced on average at the mean-field level . In the slave fermion formulation of localized spins, the spin-spin interactions of the Kondo-Heisenberg Hamiltonian become 4-fermion interaction terms:

$$\boldsymbol{s}_i \cdot \boldsymbol{S}_i = -\frac{1}{4} \left[\left(c^\dagger_{i\alpha} f_{i\alpha} \right) \left(f^\dagger_{i\beta} c_{i\beta} \right) + H.c. \right] + \frac{1}{4}, \tag{6}$$

$$\boldsymbol{S}_i \cdot \boldsymbol{S}_j = -\frac{1}{4} \left[\left(f^\dagger_{i\alpha} f_{j\alpha} \right) \left(f^\dagger_{j\beta} f_{i\beta} \right) + H.c. \right] + \frac{1}{4}, \tag{7}$$

where the sum over the spin indices is understood. A mean-field formulation can be obtained by decoupling Kondo and Heisenberg interaction terms in the Kondo and RVB channels respectively[15]:

$$\begin{aligned} \hat{H}_{MF} = & -t \sum_{\langle ij \rangle \alpha} (c^\dagger_{i\alpha} c_{j\alpha} + H.c.) + b_\infty \sum_{i\alpha} (c^\dagger_{i\alpha} f_{i\alpha} + H.c.) \\ & + \chi \sum_{\langle ij \rangle \alpha} (f^\dagger_{i\alpha} f_{j\alpha} + H.c.) \end{aligned} \tag{8}$$

The subscript ∞ in b_∞ is because we are going to generalize above Hamiltonian to the Kondo-vortex configuration. b_∞ is going to be the Kondo amplitude far away from the vortex core.

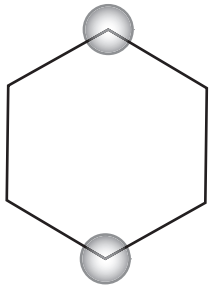

FIG. 4: The Brillouin zone of the honeycomb lattice. Corners of the Brillouin zone are where the tight-binding gap vanishes. The *independent* low-energy modes are denoted by the filled-circles around the two Dirac nodes $\pm \boldsymbol{k}_D$. The energy bands (for the c and f tight binding bands and for the mixed bands) near these two points are given in Fig. 5.

Let us first start with the c and f hopping (the first and third term) part of the Hamiltonian $\hat{H}_{MF}$. As is well-known in the honeycomb lattice, the tight-binding bands touch at the 6 corners of the Brillouin zone (see Fig. 4). At half-filling fermi surface shrinks to these 6 points, and the independent low energy modes lie near the 2 independent nodes $\pm \boldsymbol{k}_D$ shown schematically in Fig. 4. These are known as the Dirac nodes due to the relativistic structure of the low energy Lagrangian. The band structure of c and f kinetic terms near these Dirac points are therefore characterized by velocities (see Fig. 5):

$$v_c = 3t/2, \tag{9}$$

$$v_f = 3\chi/2. \tag{10}$$

For $b_\infty \neq 0$, c and f bands mix and a gap will be opened. The mixed energy levels near the Dirac nodes is given by $E_{cf}(q) = \pm \left((v_c - v_f)q \pm \sqrt{(v_f + v_c)^2 q^2 + (2b_\infty)^2} \right)/2$. The gap at the Dirac points ($q = 0$) is $2b_\infty$, but as can be seen in Fig. 5 (when $v_c \neq v_f$) the minimum gap is not located at Dirac points and is less than $2b_\infty$.

We note[20] that the sign of χ/t has to be positive for the Kondo gap to open up. For $\chi/t < 0$ we end up with a Fermi *ring* around the Dirac nodes (see Eq. (33) of Ref. 20). This sign can be gauged away at the expense of a non-uniform $b_i = (-1)^i b_\infty$, i.e. a b that alternates in sign from A to B sublattices. The $b_i = (-1)^i b_\infty$ configurations – though irrelevant for the remaining of the paper – is a simple example to emphasize that a non-uniform b can cause the spectrum to change very dramatically: from a gapped spectrum to a spectrum with infinitely many low energy excitation! Kondo vortices – the focus of this paper – is another class of non-uniform b configurations.

The established approach for the study of phase transition out of the Kondo phase is to construct a large N Lagrangian to justify the mean-field in the $N \to \infty$ limit. After this construction the self-consistent mean-field b_∞ is obtained, and the point where b_∞ vanishes is

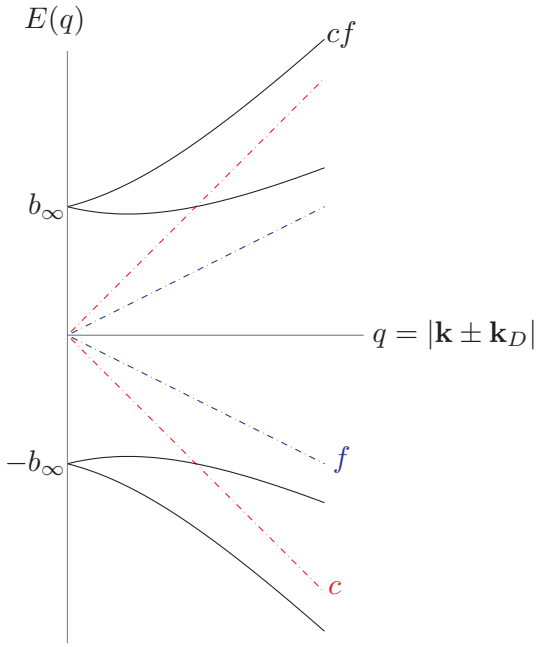

FIG. 5: Energy bands of the mean-field Hamiltonian near the Dirac nodes $\pm\boldsymbol{k}_D$. Near the Dirac nodes the energy spectrum just depends on $q = |\boldsymbol{k} \pm \boldsymbol{k}_D|$. The red dashed bands are for the conduction electrons c: $E_c(q) = \pm v_c q$, where $v_c = 3t/2$. The blue dashed bands are for the slave fermions f: $E_f(q) = \pm v_f q$, where $v_f = 3\chi/2$. The black bands are the mized bands, i.e. when $b_\infty \neq 0$: $E_{cf}(q) = \pm\left((v_c - v_f)q \pm \sqrt{(v_f + v_c)^2 q^2 + (2b_\infty)^2}\right)/2$.

the Kondo transition point. The critical properties near the transition point is studied using the renormalization group machinery, where $1/N$ serves as the small parameter controlling the expansion. We followed this route in Ref. 20 and studied the critical theory of the Kondo insulator phase of Fig. 5 to an algebraic spin liquid, as the phase transition of a Kondo phase to an algebraic spin liquid is of current interest.[9,21] Of course the main problem with this approach is is that it is only fully justified in the large N limit. The qualitative picture the large N expansion gives might extend to smaller N. However it is not at all clear if the large N expansion gives a useful qualitative picture for the heavy fermion QCP, and the main reason one would resort to large N is because the $N = 2$ problem is intractable.

However in this paper we use the simplicity the half-filled honeycomb lattice provides to approach the $N = 2$ problem directly and we go beyond the mean-field (large N) treatment of the Kondo problem. We do this by extending the $\hat{H}_{MF}$ to a more general quadratic Hamiltonian $\hat{H}_2$:

$$\begin{aligned}\hat{H}_2 = &-t\sum_{\langle ij\rangle\alpha}(c^\dagger_{i\alpha}c_{j\alpha} + H.c.)\\ &+\chi\sum_{\langle ij\rangle\alpha}(e^{ia_{ij}}f^\dagger_{i\alpha}f_{j\alpha} + H.c.)\\ &+\sum_{i\alpha}(b_i c^\dagger_{i\alpha}f_{i\alpha} + H.c.),\end{aligned} \tag{11}$$

where we have relaxed the condition of a unform b_i field and a zero-flux a_{ij} configuration. We note here that in writing $\hat{H}_{MF}$, and $\hat{H}_2$ we ignored the chemical potential terms

$$\hat{H}_\mu = -\mu^c(\sum_{i\alpha}c^\dagger_{i\alpha}c_{i\alpha} - \mathcal{N}) - \sum_i \mu^f_i(f^\dagger_{i\alpha}f_{i\alpha} - 1), \tag{12}$$

where $\mathcal{N}$ is the number of lattice sites. In Appendix A we show that the chemical potentials μ^c and μ^f_i are indeed zero in the half-filled case.

A general b_i and a_{ij} configuration can be seen as an *excitation* over the uniform mean-field case, as the total energies of the occupied states will be larger than the uniform mean-field configuration. The uniform mean-field case in the honeycomb lattice was studied in Ref. 20, and it was shown that the KI phase is stabilized for any $J_H \geq 0$ beyond a finite Kondo coupling J^c_K. As far as the mean-field case is concerned, the role of Heisenberg coupling J_H is to push the critical Kondo coupling to larger values as it is increased. We emphasize that the study of these configurations (i.e. "exciation fields") can be fruitful for any Kondo lattice model, and their proliferation may lead to interesting phases.

Here we focus on a class of these exciation configurations we call Kondo vortices. They are identified in continuum limit as $b(\boldsymbol{r}) = |b(r)|e^{\pm i\theta(\boldsymbol{r})}$, where $|b(r)| \propto r$ as $r \to 0$ and converges to the mean-field value b_∞ as $r \to \infty$. Furthermore due to the presence of $|(\partial_\mu + ia_\mu)b|^2$ in the action[20] (which is dictated on gauge-invariance ground), the finite energy configurations are obtained by inserting a $\mp 2\pi$ gauge flux extended around the vortex core.[17,18] An example of such a configuration is

$$b(\boldsymbol{r}) = b_\infty \tanh(r/\xi_b)e^{+i\theta(\boldsymbol{r})}, \tag{13}$$

$$a_\theta(r) = -\tanh^2(r/\Lambda)/r, \tag{14}$$

where the following gauge

$$\boldsymbol{a}(\boldsymbol{r}) = a_\theta(r)\hat{\boldsymbol{\theta}} \tag{15}$$

is chosen for the gauge field. Now that we have defined the Kondo vortex configuration we are going to study how it affects the energy spectrum.

III. ZERO MODES IN THE PRESENCE OF A KONDO VORTEX

The KV excitation is special since in its presence 4 *zero* modes appear right at the *chemical potential* in the KI

phase. In the approach we have taken, the zero modes will later play a big role in giving a spin-1 structure to our Kondo vortices. In the absence of zero modes we are forced to occupy the Dirac sea with up and down spins and the resulting state would be a magnetically featureless spin singlet state.

We first analyze the zero mode equations in the continuum limit. To find the zero modes we expand the Hamiltonian near the Dirac nodes, and set energy=0. The quadratic Hamiltonian of Eq. (8) near $\pm \boldsymbol{k}_D$ node is given by the following matrix

$$\mathcal{H}_{\pm} = \begin{pmatrix} v_c(q_1\tau_2 \pm q_2\tau_1) & b \\ b^* & -v_f[(q_1+a_1)\tau_2 \pm (q_2+a_2)\tau_1] \end{pmatrix}, \tag{16}$$

where $\boldsymbol{a} = a_1\hat{\boldsymbol{x}} + a_2\hat{\boldsymbol{y}}$ is the spatial component of the gauge field, and τ_μ are Pauli matrices acting on the AB flavors. The zero mode equations is therefore given by

$$\mathcal{H}_{\pm}\pi_{\pm} = 0, \tag{17}$$

where $\pi_\pm$ is the column vector

$$\pi_{\pm} = \begin{pmatrix} c_{A\pm} \\ c_{B\pm} \\ f_{A\pm} \\ f_{B\pm} \end{pmatrix}. \tag{18}$$

In Appendix B we analyze the zero mode equations in real space after replacing $q_j = i\partial_j$. There are 2×2 zero modes labeled by their $\{+,-\}$ Dirac node and $\{\uparrow,\downarrow\}$ spin flavors. The energy spectrum of the mean-field state and in the presence of the vortex is shown schematically in Fig. 6.

Next we analyze the energy spectrum of the *lattice* Hamiltonian of Eq. (11) in the presence of a KV. We use a "ring" geometry – an example of which is given in Fig. 7. The center of the figure is the $r = 0$ point. b_i for each lattice site is then obtained using the continuum limit expression given in Eq. (13) by replacing $\boldsymbol{r}$ with $\boldsymbol{r}_i$. We spread the 2π flux uniformly over a N_Λ number of rings, and find a_{ij}'s that enclose the needed flux per plaquette. Since in the KI phase $b_\infty \neq 0$ different gauge choices to enclose the flux results in different spectrums - however they all lead to emergence of 4 zero modes as one takes the number of rings $N_r \to \infty$.

We can imagine an adiabatic process on the lattice where the zero modes are created adiabtically as one gradually inserts the vortex. This is done by introducing the parameters κ_1 and κ_2, where we consider enclosing $2\pi\kappa_1$ flux and also take $b_i = |b_i|e^{i\kappa_2\theta_i}$. In Fig. 8 we consider the case $\kappa_1 = \kappa_2$ in the $[0,1]$ interval. This artificial way of adiabatically inserting the flux (apart from showing the gradual emergence of zero modes) will be useful to elaborate on some conceptual points in the next section.

In Fig. 9, we have also provided the finite size scaling plot of the closest energy to the zero ε_0 as function of $1/N_r$, which is a very convincing evidence for the existence of the zero modes: $\varepsilon_0 \to 0$ as $N_r \to \infty$. This

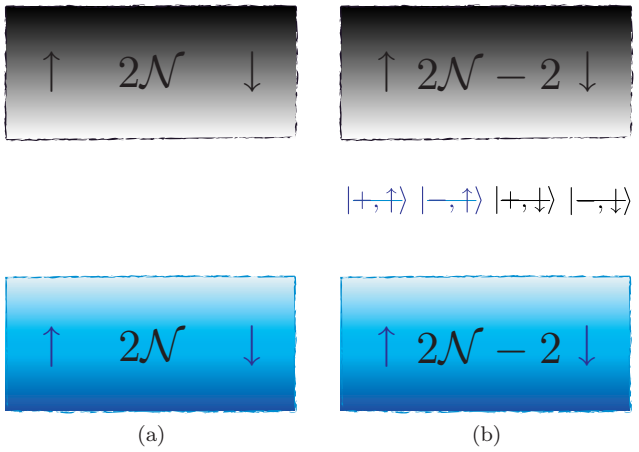

FIG. 6: 6(a) The *schematic* figure of the energy levels of the mean-field Hamiltonian of Eq. (8). The occupied states are colored by blue. $\mathcal{N}$ is the number of lattice sites. There are two types of fermions $\{c, f\}$, and two spin flavors $\{\uparrow,\downarrow\}$ – therefore $4\mathcal{N}$ states in total, half of which is occupied. 6(b) The schematic figure of the energy levels of the Hamiltonian of Eq. (11) in the presence of a KV background. 2 states from the Dirac sea and 2 states form the unoccupied states are brought to *zero* energy, where the chemical potential is located. Due to charge conservation half of these 4 zero modes has to be occupied. An example of this zero mode occupation is shown in this figure. There are $(4\times 3)/2$ ways to occupy these zero modes. We later classify this 6 ways of occupying zero modes as 3 spin-triplet nodal-singlet, plus 3 spin-singlet nodal-triplet states.

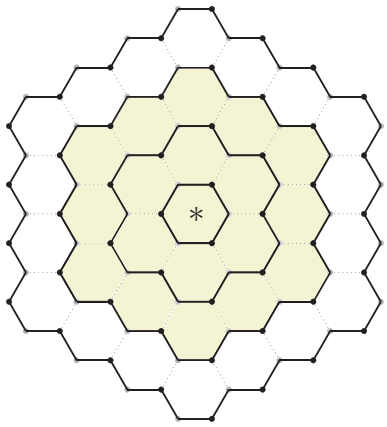

FIG. 7: An example of a gauge-symmetric (ring) geometry (with N_r number of rings) to study the energy spectrum of the Hamiltonian $\hat{H}_2$ [Eq. (11)] and to find how $v_\xi^{i\dagger}$ [Eq. (21)] transforms under the $\pi/3$ rotation around the center of the plaquette labeled $*$. The bold links are the links where the gauge field is non-zero. We let the 2π flux to spread uniformly over N_Λ number of rings, and choose a symmetric gauge to enclose the flux. The numerics is done in the *open* boundary condition. Plaquettes with non-zero flux passing through them are shaded with yellow. In this figure $N_r = 4, N_\Lambda = 3$.

continuum limit is going to be discussed further in Appendix B. We have also confirmed that a KV with $2\pi n$

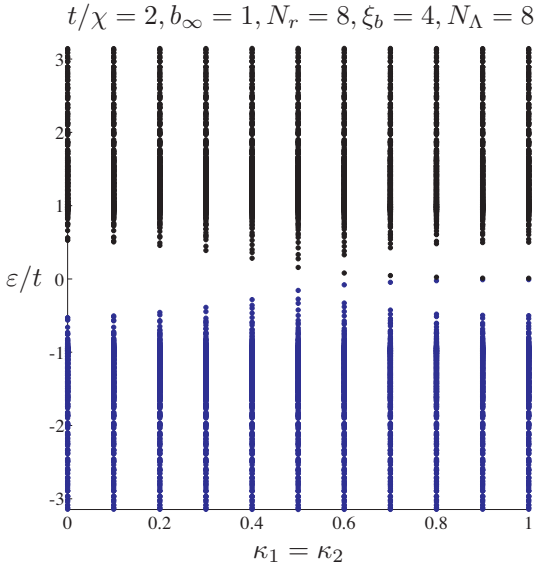

FIG. 8: The evolution of energy levels ε (in units of t), as a function of κ for one spin flavor. κ_1 is a fraction of 2π flux enclosed, and κ_2 characterizes the phase "twist" of the b field $b_i = |b_i|e^{i\kappa_2\theta_i}$. They are parameters to control the evolution of the spectrum from mean-field state ($\kappa_1 = \kappa_2 = 0$) to the KV state ($\kappa_1 = \kappa_2 = 1$). In the example shown here we vary $\kappa_1 = \kappa_2$ in the $[0, 1]$ interval.

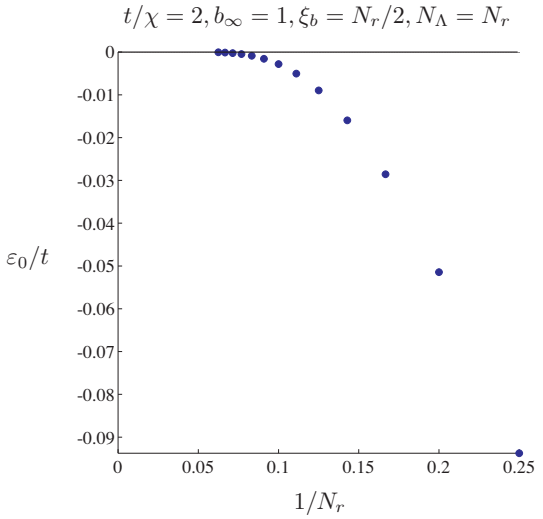

FIG. 9: ε_0 is the nearest energy in the Dirac sea to the chemical potential (i.e. *zero* energy). ε_0 is plotted (in units of t) as a function of $1/N_r$, where N_r is the number of rings in the geometry we used for our numerics (See Fig. 7). $\varepsilon_0 \to 0$ in the continuum limit $N_r \to \infty$.

phase twist in the b field has n zero modes per node and per spin flavor, a property that we would expect on topological grounds.

IV. SPIN-1 VORTEX OPERATORS

After establishing the zero modes, we can now discuss the construction of a spin-1 vortex creation operator. We define vortex creation operators as operators that *increase* the gauge flux by 2π. If we only limit ourselves with states that are connected to the mean-field state, the 2π flux-increasing operator contains two terms:

$$m^{+\dagger}_{(a\alpha)(b\beta)} = z^{+\dagger}_{a\alpha} z^{+\dagger}_{b\beta} \left|DS,+\right\rangle \left\langle G\right|, \tag{19}$$

$$m^{-\dagger}_{(a\alpha)(b\beta)} = \left|G\right\rangle \left\langle DS,-\right| z^{-}_{b\beta} z^{-}_{a\alpha}, \tag{20}$$

where $a, b \in \{+,-\}$ are nodal, and $\alpha, \beta \in \{\uparrow,\downarrow\}$ are spin flavors. $|G\rangle$ is the MF ground state, $|DS+\rangle$ is the Dirac sea of *negative* energy states in the presence of the $+2\pi$ gauge flux, $z^{+\dagger}_{a\alpha}$ is the zero mode creation operator (with $a\alpha$ flavor) for the state with $+2\pi$ gauge flux, and $z^{-}_{a\alpha}$ is the zero mode annihilation operator for the state with -2π gauge flux. In words what $m^{+\dagger}_{(a\alpha)(b\beta)}$ does is to add a 2π vortex to the mean-field state, and what $m^{-\dagger}_{(a\alpha)(b\beta)}$ does is to add a 2π flux to the -2π vortex state thus bringing it back to the ground state. They both have the effect of adding a 2π flux, therefore a 2π flux vortex creation operator should contain both terms. There are $\frac{4\times3}{2}$ ways to occupy the zero modes. We classify these 6 KV creation operators into spin-triplet nodal-singlet operators $v^{i\dagger}_\xi$, and spin-singlet nodal-triplet operators $u^{i\dagger}_\xi$:

$$\begin{aligned} v^{i\dagger}_\xi = &\left[(i\sigma^2)\sigma^i\right]_{\alpha\beta}(i\mu^2)_{ab} m^{+\,\dagger}_{(a\alpha)(b\beta)} \\ &+ \xi\left[\sigma^i(i\sigma^2)\right]_{\alpha\beta}(i\mu^2)_{ab} m^{-\,\dagger}_{(a\alpha)(b\beta)} \end{aligned} \tag{21}$$

$$\begin{aligned} u^{i\dagger}_\xi = &\left[(i\mu^2)\mu^i\right]_{ab}(i\sigma^2)_{\alpha\beta} m^{+\,\dagger}_{(a\alpha)(b\beta)} \\ &+ \xi\left[\mu^i(i\mu^2)\right]_{ab}(i\sigma^2)_{\alpha\beta} m^{-\,\dagger}_{(a\alpha)(b\beta)} \end{aligned} \tag{22}$$

Since we are interested in the magnetically ordered phases that can arise by condensing Kondo vortices we focus on $v^{i\dagger}_\xi$ operators. From

$$\begin{aligned} &\left(\left[(i\sigma^2)\sigma^i\right]_{\alpha\beta}(i\mu^2)_{ab} m^{+\,\dagger}_{(a\alpha)(b\beta)}\right)^\dagger \\ &= \left[(i\sigma^2)(\sigma^i)^*\right]_{\alpha\beta}(i\mu^2)_{ab} m^{+}_{(a\alpha)(b\beta)} \\ &= -\left[\sigma^i(i\sigma^2)\right]_{\alpha\beta}(i\mu^2)_{ab} m^{+}_{(a\alpha)(b\beta)}, \end{aligned} \tag{23}$$

v^i_ξ is given by

$$\begin{aligned} v^{i}_\xi = &-\left[\sigma^i(i\sigma^2)\right]_{\alpha\beta}(i\mu^2)_{ab} m^{+}_{(a\alpha)(b\beta)} \\ &- \xi^*\left[(i\sigma^2)\sigma^i\right]_{\alpha\beta}(i\mu^2)_{ab} m^{-}_{(a\alpha)(b\beta)} \end{aligned} \tag{24}$$

The proof that $v^{i\dagger}_\xi$ transforms like a spin 1 under $SU(2)$ spin rotation is straightforward. Let us assume a $SU(2)$ spin rotation with angle $2\boldsymbol{\phi}$:

$$c^\dagger_{a\alpha} \to c^\dagger_{a\alpha'}(e^{-i\boldsymbol{\phi}\cdot\boldsymbol{\sigma}})_{\alpha'\alpha} \tag{25}$$

Under this transformation

$$\begin{aligned}
&\left[(i\sigma^2)\sigma^i\right]_{\alpha\beta} m^{+\dagger}_{(a\alpha)(b\beta)} \rightarrow \\
&[\sigma^i(i\sigma^2)]_{\alpha\beta}(e^{-i\boldsymbol{\phi}\cdot\boldsymbol{\sigma}})_{\beta'\beta}(e^{-i\boldsymbol{\phi}\cdot\boldsymbol{\sigma}})_{\alpha'\alpha} m^{+\dagger}_{(a\alpha')(b\beta')} \\
&= [e^{-i\boldsymbol{\phi}\cdot\boldsymbol{\sigma}}\sigma^i(i\sigma^2)e^{-i\boldsymbol{\phi}\cdot\boldsymbol{\sigma}^T}]_{\alpha'\beta'} m^{+\dagger}_{(a\alpha')(b\beta')} \\
&= [e^{-i\boldsymbol{\phi}\cdot\boldsymbol{\sigma}}\sigma^i e^{+i\boldsymbol{\phi}\cdot\boldsymbol{\sigma}}\ (i\sigma^2)]_{\alpha\beta} m^{+\dagger}_{(a\alpha)(b\beta)},
\end{aligned} \tag{26}$$

which is to say $v^{i\dagger}_\xi$ rotates as a spin-1 under $SU(2)$ spin flavor rotations. The invariance of $v^{i\dagger}_\xi$ under nodal rotations (with angle $2\boldsymbol{\theta}$) is also given below:

$$\begin{aligned}
&[(i\mu^2)]_{ab} m^{+\dagger}_{(a\alpha)(b\beta)} \\
&\rightarrow [(i\mu^2)]_{ab}(e^{-i\boldsymbol{\phi}\cdot\boldsymbol{\mu}})_{b'b}(e^{-i\boldsymbol{\phi}\cdot\boldsymbol{\mu}})_{a'a} m^{+\dagger}_{(a'\alpha)(b'\beta)} \\
&= [e^{-i\boldsymbol{\theta}\cdot\boldsymbol{\mu}}(i\mu^2)e^{-i\boldsymbol{\theta}\cdot\boldsymbol{\mu}^T}]_{a'b'} m^{+\dagger}_{(a'\alpha)(b'\beta)} \\
&= [e^{-i\boldsymbol{\theta}\cdot\boldsymbol{\mu}}e^{+i\boldsymbol{\theta}\cdot\boldsymbol{\mu}}\ (i\mu^2)]_{ab} m^{+\dagger}_{(a\alpha)(b\beta)} \\
&= [(i\mu^2)]_{ab} m^{+\dagger}_{(a\alpha)(b\beta)}.
\end{aligned} \tag{27}$$

This finishes our discussion of classifying KV creation operators.

V. KONDO VORTEX TRANSFORMATIONS

In this section we study how $v^{i\dagger}_\xi$ transforms under various symmetry transformations of the quadratic Hamiltonian $\hat{H}_2$ of Eq. (11). We already know that condensation of $v^{i\dagger}_\xi$ leads to *a* magnetic phase, since it picks a direction and breaks the $SU(2)$ spin rotation symmetry. We however would like to know what kind of a magnetic phase it is. The strategy is to find out the transformation properties of $v^{i\dagger}_\xi$, and compare them with the transformation properties of various magnetically ordered states under various symmetry operations. This method has been used beforehand for the studying the effect of instantons in the gapless phase of the $U(1)$ algebraic spin liquid.[22–24]

Some symmetry transformation generators of the Hamiltonian $\hat{H}_2$ is given in Table I. We have not explicitly written the transformations under reflection and translations, as they act exactly like $\mathcal{R}^*_{\pi/3}$– in that they only act on the site indices $i \rightarrow i'$.

We note that that the definition of $v^{i\dagger}_\xi$ is only well-defined if the phases of single particle states of the mean-field states are locked to their counterparts in the vortex state. A simple way to guarantee this phase locking is through the "artificial" adiabatic process outline in the previous section (see Fig. 8).

Now we are going to discuss how $v^{i\dagger}_\xi$ trasnform under time-reversal $\mathcal{T}$, charge-conjugation $\mathcal{C}$, rotation $\mathcal{R}^*_{\pi/3}$, and translations $T_{\boldsymbol{a}_i}$.

	$c_{i\alpha}$	$f_{i\alpha}$	b_i	a_{ij}
$\mathcal{T}$	$(i\sigma^2)_{\alpha\beta}c_{i\beta}$	$(i\sigma^2)_{\alpha\beta}f_{i\beta}$	b^*_i	$-a_{ij}$
$\mathcal{C}$	$\epsilon_i(i\sigma^2)_{\alpha\beta}c^\dagger_{i\beta}$	$-\epsilon_i(i\sigma^2)_{\alpha\beta}f^\dagger_{i\beta}$	b^*_i	$-a_{ij}$
$\mathcal{R}^*_{\pi/3}$	$c_{i'\alpha}$	$f_{i'\alpha}$	$b_{i'}$	$a_{i'j'}$

TABLE I: The table of the transformation of lattice fields under time-reversal $\mathcal{T}$, charge-conjucation $\mathcal{C}$, and a $\pi/3$ rotation around the center of a plaquette (labeled $*$) $\mathcal{R}^*_{\pi/3}$. Primed i' etc, is just the transformed index under $\mathcal{R}^*_{\pi/3}$. Other lattice space-group transformations (translations, rotations, and reflections) acts in the same way as in $\mathcal{R}^*_{\pi/3}$ – in that they only act on the site indices $i \rightarrow i'$.

A. Time reversal

From the transformation $b_i \rightarrow b^*_i$, and $a_{ij} \rightarrow -a_{ij}$ under time-reversal, it is clear that $\mathcal{T}$ send any state in the + KV configuration to its corresponding state in − KV, in addition to rotating its spin according to $(i\sigma^2)$ factor in Table I:

$$\begin{aligned}
\mathcal{T}: &z^{+\dagger}_{a\alpha} z^{+\dagger}_{b\beta} \left|DS,+\right\rangle \left\langle G\right| \rightarrow \\
&(i\sigma^2)_{\alpha\alpha'}(i\sigma^2)_{\beta\beta'} z^{-\dagger}_{a\alpha'} z^{-\dagger}_{b\beta'} \left|DS,-\right\rangle \left\langle G\right|,
\end{aligned} \tag{28}$$

Therefore the first term of $v^{i\dagger}_\xi$ [Eq. (21)] transforms to:

$$\begin{aligned}
&\mathcal{T}: [(i\sigma^2)\sigma^i]_{\alpha\beta}(i\mu^2)_{ab} m^{+\dagger}_{(a\alpha)(b\beta)} \\
&\rightarrow [(i\sigma^2)(\sigma^i)^*]_{\alpha\beta}(i\mu^2)_{ab}(i\sigma^2)_{\alpha\alpha'}(i\sigma^2)_{\beta\beta'} m^{-}_{(a\alpha')(b\beta')} \\
&= \left[-(i\sigma^2)(i\sigma^2)(\sigma^i)^*(i\sigma^2)\right]_{\alpha'\beta'}(i\mu^2)_{ab} m^{-}_{(a\alpha')(b\beta')} \\
&= -[(i\sigma^2)\sigma^i]_{\alpha\beta}(i\mu^2)_{ab} m^{-}_{(a\alpha)(b\beta)}.
\end{aligned} \tag{29}$$

Similar algebra for the second term results in

$$\begin{aligned}
\mathcal{T}: v^{i\dagger}_\xi \rightarrow &-\left[(i\sigma^2)\sigma^i\right]_{\alpha\beta}(i\mu^2)_{ab} m^{-}_{(a\alpha)(b\beta)} \\
&-\xi^*\left[\sigma^i(i\sigma^2)\right]_{\alpha\beta}(i\mu^2)_{ab} m^{+}_{(a\alpha)(b\beta)}
\end{aligned} \tag{30}$$

We demand that under time reversal $v^{i\dagger}_\xi$ transforms to v^i_ξ except for a possible phase factor. Comparing the above equation with v^i_ξ given in Eq. (24) results in $\xi^{*2} = 1$. Therefore vortex creation operators are classified by their transformation under time reversal – they can only be either odd or even under time reversal:

$$\mathcal{T}: \boldsymbol{v}^\dagger_\pm \rightarrow \pm\boldsymbol{v}_\pm. \tag{31}$$

B. Charge conjugation

To find how $\boldsymbol{v}^\dagger_\pm$ transforms under charge-conjugation, let us first define $\gamma^{+\dagger}_{\varepsilon\alpha}$ as the creation operator of the

states with energy ε with spin α and in the presence of + KV. The expansion of $\gamma^{+\dagger}_{\varepsilon\alpha}$ is given by:

$$\gamma^{+\dagger}_{\varepsilon\alpha} = \sum_i C^+_{\varepsilon i} c^\dagger_{i\alpha} + F^+_{\varepsilon i} f^\dagger_{i\alpha}, \tag{32}$$

where $C^+_{\varepsilon i}$, and $F^+_{\varepsilon i}$ are complex numbers which are obtained by the looking at the eigenvectors of the Hamiltonian matrix $\hat{H}_2$ with eigenvalue ε. Let us also define $\tilde{\gamma}^{+\dagger}_{\varepsilon\alpha}$, derived from $\gamma^{+\dagger}_{\varepsilon\alpha}$

$$\tilde{\gamma}^{+\dagger}_{\varepsilon\alpha} := \sum_i \epsilon_i C^+_{\varepsilon i} c^\dagger_{i\alpha} - \epsilon_i F^+_{\varepsilon i} f^\dagger_{i\alpha}, \tag{33}$$

where $\epsilon_i = (-)^i$, that is to say, it is -1 on A sublattices, and is $+1$ on B sublattices of the honeycomb lattice. In Appendix A we show that

$$\tilde{\gamma}^{+\dagger}_{\varepsilon\alpha} = \gamma^{+\dagger}_{-\varepsilon\alpha}. \tag{34}$$

Under charge conjugation (see Table II):

$$C : \gamma^{+\dagger}_{\varepsilon\alpha} \to (i\alpha^2)_{\alpha\beta}\tilde{\gamma}^{+*}_{\varepsilon\beta} = (i\sigma^2)_{\alpha\beta}\gamma^{+*}_{-\varepsilon\beta} = (i\sigma^2)_{\alpha\beta}\gamma^{-}_{-\varepsilon\beta}. \tag{35}$$

In words (in addition to $(i\sigma^2)_{\alpha\beta}$ spin rotation) charge conjugation sends the particle *creation* operators in the Dirac sea of a + vortex to the *destruction* operators of the unoccupied states of the − vortex. However since charge conjugation also sends the empty (vacuum) state to the *fully* occupied state the net effect is to send Dirac sea of + vortex to the Dirac sea of − vortex. For the zero modes this involves two spin flips one coming from the $(i\sigma^2)_{\alpha\beta}$ factor in the definition of the charge conjucation, and other for going from occupied states to unoccupied states. Therefore the first term of $v^{i\dagger}_\xi$ transforms to:

$$\begin{aligned} \mathcal{C} : &[(i\sigma^2)\sigma^i]_{\alpha\beta}(i\mu^2)_{ab} m^{+\dagger}_{(a\alpha)(b\beta)} \\ &\to [(i\sigma^2)(\sigma^i)]_{\alpha\beta}(i\mu^2)_{ab} m^{-}_{(a\alpha)(b\beta)}. \end{aligned} \tag{36}$$

Similar algebra for the second term results in

$$\begin{aligned} \mathcal{C} : v^{i\dagger}_\xi \to &[(i\sigma^2)\sigma^i]_{\alpha\beta}(i\mu^2)_{ab} m^{-}_{(a\alpha)(b\beta)} \\ &+ \xi \left[\sigma^i(i\sigma^2)\right]_{\alpha\beta}(i\mu^2)_{ab} m^{+}_{(a\alpha)(b\beta)}. \end{aligned} \tag{37}$$

Compare this with v^i_ξ [Eq. (24)] for $\xi = \pm 1$:

$$\mathcal{C} : \boldsymbol{v}^\dagger_\pm \to \mp \boldsymbol{v}_\pm. \tag{38}$$

C. Rotation $\mathcal{R}^*_{\pi/3}$, and Translations $T_{\boldsymbol{a}_i}$

To obtain the transformation of $v^{i\dagger}_\xi$ under $\mathcal{R}^*_{\pi/3}$ we resort to numerics. This is done by diagonlizaing the Hamiltoniain $\hat{H}_2$ in a ring geometry (See Fig. 7) using a symmetric gauge. Each single particle state is then transformed according to $\mathcal{R}^*_{\pi/3}$. Let us take the column vector corresponding to the single particle state with energy ε (where we ignore the vortex $\pm$, and spin index since rotation does not change the vorticity or spin) :

$$|\varepsilon\rangle = [C_1 \cdots C_{\mathcal{N}} F_1 \cdots F_{\mathcal{N}}]^T, \tag{39}$$

and $\mathcal{N}$ is the number of sites. Under $\mathcal{R}^*_{\pi/3}$, $|\varepsilon\rangle$ transforms to

$$\mathcal{R}^*_{\pi/3} : |\varepsilon\rangle \to [C_{1'} \cdots C_{\mathcal{N}'} F_{1'} \cdots F_{\mathcal{N}'}]^T, \tag{40}$$

where i' the index of the lattice site obtained by rotating lattice site with index i. In a symmetric gauge the transformed $|\varepsilon\rangle$ is going to be proportional to $|\varepsilon\rangle$ except for a uniform phase factor on the weights for f orbitals:

$$|\varepsilon\rangle \to e^{i\theta_\varepsilon}[C_1 \cdots C_{\mathcal{N}} e^{i\pi/3} F_1 \cdots e^{i\pi/3} F_{\mathcal{N}}]^T. \tag{41}$$

The $e^{i\pi/3}$ phase factor is the trivial phase to compensate the constant $\pi/3$ shift in the phase of the b field. Transformed $v^{i\dagger}_\xi$ is then obtained by multiplying all the $e^{i\theta_\varepsilon}$ phase factors of the single-particle states that make up $v^{i\dagger}_\xi$ [See Eq. (19)– (21)]. We find

$$\mathcal{R}^*_{\pi/3} : v^{i\dagger}_\xi \to -v^{i\dagger}_\xi. \tag{42}$$

The minus sign above is independent of lattice sizes and vortex configurations! This is quite a nontrivial result as all the states in the Dirac sea and 2 zero modes contribute to this *minus* sign.

To find how $v^{i\dagger}_\xi$ transforms under lattice translations we use the following identity in the honeycomb lattice

$$R^*_{\pi/3} T_{\boldsymbol{a}_1} T_{\boldsymbol{a}_2} R^{*-1}_{\pi/3} T^{-1}_{\boldsymbol{a}_2} = 1, \tag{43}$$

where $\boldsymbol{a}_1 = (0, \sqrt{3})$, and $\boldsymbol{a}_2 = (-3/2, -\sqrt{3}/2)$ in the units of nearest neighbor links. Demanding $\boldsymbol{v}^\dagger_\xi$ to be an eigenvector of $T_{\boldsymbol{a}_i}$ results in

$$T_{\boldsymbol{a}_1} : \boldsymbol{v}^\dagger_\xi \to \boldsymbol{v}^\dagger_\xi \tag{44}$$

The same result holds for $T_{\boldsymbol{a}_2}$.

	$\boldsymbol{v}^\dagger_\pm$	$\boldsymbol{v}_\pm + \boldsymbol{v}^\dagger_\pm$	$i(\boldsymbol{v}_\pm - \boldsymbol{v}^\dagger_\pm)$	$i\boldsymbol{v}_\pm \times \boldsymbol{v}^\dagger_\pm$
$\mathcal{T}$	$\pm\boldsymbol{v}_\pm$	$\pm$	$\pm$	$+$
$\mathcal{C}$	$\mp\boldsymbol{v}_\pm$	$\mp$	$\pm$	$-$
$\mathcal{R}^*_{\pi/3}$	$-\boldsymbol{v}^\dagger_\pm$	$-$	$-$	$+$
$T_{\boldsymbol{a}_i}$	$+\boldsymbol{v}^\dagger_\pm$	$+$	$+$	$+$

TABLE II: The table of the transformation of the spin-1 vortex creation operator $\boldsymbol{v}^\dagger_\xi$, and 3 Hermitian operators constructed from it. Time reversal dictates ξ to be either ± 1.

It would have been ideal to also find the transformation of $\boldsymbol{v}^\dagger_\xi$ under lattice reflections. The problem in using the numerics – the way we used it for studying the action of $\mathcal{R}^*_{\pi/3}$ on vortex operators – is that reflections change vortices to anti-vortices. We note that in diagonalizing the

Hamiltonian $\hat{H}_2$ there is an arbitrary phase associated with each single particle state. The arbitrary phase $e^{i\vartheta}$ for the + vortex state, appears as $e^{-i\vartheta}$ in the − vortex state and causes an arbitrary $e^{2i\vartheta}$ phase accumulation! This problem could have been circumvented by locking the phase of each single particle state with its "corresponding" state in the mean-field spectrum. However we do not have a way of "locking" these phases, and therefore can not trust our numerical results for reflections.

The results of the symmetry transformations we studied are summarized in table II. We see that $\mathrm{Re}(\boldsymbol{v}_-) = \boldsymbol{v}_- + \boldsymbol{v}_-^\dagger$ transforms identically to the standard two sublattice antiferromagnetic Neel order parameter. Thus its condensation will lead to the usual Neel order. In the next section we discuss the nature of the AF phase transition mediated by the condensation of the $\mathrm{Re}(\boldsymbol{v}_-)$.

VI. KONDO VORTEX CONDENSATION AND THE $O(3)$ TRANSITION

In this section we discuss the universality class of the AF phase transition mediated by the KV condensation. To describe the *universality* of the resulting AF phase transition it is convenient to pass to a dual description[25,26] directly in terms of the Kondo vortices. As the Kondo hybridization field b is coupled to a gauge field, its vortices do not have any long range interactions. The dual free energy may then be readily written down by demanding invariance under all physical symmetries and is given by:

$$F = \sum_{\xi=\pm 1} \Big(t_\xi |\boldsymbol{v}_\xi|^2 + r_\xi (\boldsymbol{v}_\xi^2 + \boldsymbol{v}_\xi^{*2}) + u_\xi |\boldsymbol{v}_\xi|^4 + s_\xi \boldsymbol{v}_\xi^2 \boldsymbol{v}_\xi^{*2} + w_\xi |\boldsymbol{v}_\xi \times \boldsymbol{v}_\xi^*|^2 + \cdots \Big). \tag{45}$$

We emphasize that, in contrast to the usual boson-vortex duality, due to the r_ξ terms here the vorticity is not conserved. In other words the free energy is *not* invariant under a phase rotation of the vortex fields. This is because the gauge field a_{ij} in the original description is compact. This allows for instanton configurations where the gauge flux can change in units of 2π. However the spin carried by the vortices prohibits single instanton events; pairs of vortices in a spin singlet can nevertheless be created or destroyed as described by the r_ξ term.

If $r_- < 0$, $\mathrm{Re}(\boldsymbol{v}_-)$ will condense first, while $\mathrm{Im}(\boldsymbol{v}_-)$ remains zero. We identified $\mathrm{Re}(\boldsymbol{v}_-)$ as the Neel vector, and this condensation describes the Kondo insulator to AF transition. The free energy at the transition is then given by

$$F = (t_- + r_-)\mathrm{Re}(\boldsymbol{v}_-)^2 + (u_- + s_-)\mathrm{Re}(\boldsymbol{v}_-)^4 + \cdots, \tag{46}$$

which describes an $O(3)$ transition for $\mathrm{Re}(\boldsymbol{v}_-)$. Therefore in our theoretical framework, this KV mediated AF transition is an $O(3)$ transition.

This result is perhaps not unexpected, because a charge gap exists on both sides of the AF transition and the notion of an onset of Kondo screening is an artifact of mean field theory.

VII. CONCLUSION

In this paper, we have proposed destroying the Kondo phase by proliferating Kondo vortices. To make analytical progress we have studied this proposal in the honeycomb lattice at half-filling. The particle-hole symmetry of the half-filled honeycomb lattice guarantees that the chemical potential stays at zero. The relativistic structure of the low energy modes, furthermore, has allowed us to study the Kondo vortices in the continuum limit, and to find 4 zero modes right at the chemical potential. We have shown that *spin-triplets* can be created by a Kondo vortex because of the *zero modes* it generates at the chemical potential.

This gives us a nice picture that a magnetic transition can be driven by proliferating Kondo vortices. We have also identified a class of these spin-triplets that transform like a *Néel* order. Due to the half-filled limitation of this model, however, this Kondo-vortex-driven antiferromagentic transition is in the $O(3)$ universality class.

VIII. ACKNOWLEDGMENTS

PAL was supported by the Department of Energy under grant DE-FG02-03ER46076, and TS by NSF Grant DMR-0705255.

Appendix A: Some lemmas regarding the Hamiltonian $\hat{H}_2$

In this appendix we prove a few statements which we used throughout the text. We suppress the spin flavor index α since it is not relevant. The proofs made here can be generalized to a more general Hamiltonian than $\hat{H}_2$ where $\chi e^{ia_{ij}}$ is replaced with χ_{ij}. The trasformation $a_{ij} \to -a_{ij}$ throughout this appendix should then be replaced with $\chi_{ij} \to \chi_{ij}^*$.

Lemma I. The spectrum S and $-S$ of $\hat{H}_2$ are the same. The proof is very simple as under the *unitary* transformation

$$c_i \to \epsilon_i c_i, \tag{A1}$$

$$f_i \to -\epsilon_i f_i, \tag{A2}$$

$\hat{H}_2$ transforms to

$$\hat{H}_2 \to -\hat{H}_2. \tag{A3}$$

The proof also implies Eq. (34).

Lemma II. Under vortex–antivortex transformation, i.e. the simultaneous transformation:

$$b_i \to b_i^*, \tag{A4}$$
$$a_{ij} \to -a_{ij}, \tag{A5}$$

the densities $\langle c_i^\dagger c_i\rangle$ remain unchanged:

$$\langle c_i^\dagger c_i\rangle \to \langle c_i^\dagger c_i\rangle \tag{A6}$$

That is to say $\langle c_i^\dagger c_i\rangle$ for a vortex is the same as one for an antivortex.

Proof:

$$\hat{H}_2 = \Pi^\dagger \mathbb{H} \Pi = \Gamma^\dagger \mathbb{E} \Gamma, \tag{A7}$$

where Π is the column matrix that includes both c_i and f_i: $\Pi_{i_c} = c_i$. $\mathbb{H}$ is the complex matrix corresponding to $\hat{H}_2$, and $\Gamma = U^\dagger \Pi$ are the eigen-modes (i.e. $\mathbb{E}$ is a diagonal matrix of the energy levels). Expanding $\langle c_i^\dagger c_i\rangle$ using matrix U results in:

$$\begin{aligned}\langle c_i^\dagger c_i\rangle &= U^\dagger_{m,i_c} U_{i_c,n} \langle \Gamma^\dagger_m \Gamma_n\rangle \\ &= U^\dagger_{m,i_c} U_{i_c,n} \delta_{mn} f(\varepsilon_m) \\ &= |U_{i_c,m}|^2 f(\varepsilon_m),\end{aligned} \tag{A8}$$

where $f(\varepsilon_m)$ is the fermi disdribution function. Under the transformation $\{b_i \to b_i^*, a_{ij} \to -a_{ij}\}$ we have $\{\mathbb{H} \to \mathbb{H}^* \Rightarrow U \to U^*\}$, and therefore

$$\langle c_i^\dagger c_i\rangle \to \langle c_i^\dagger c_i\rangle \tag{A9}$$

The same proof goes for f_i:

$$\langle f_i^\dagger f_i\rangle \to \langle f_i^\dagger f_i\rangle \tag{A10}$$

Lemma III. $\langle c_i^\dagger c_i\rangle$ of a vortex is the same as $1-\langle c_i^\dagger c_i\rangle$ for an antivortex. Proof: We know accompany the vortex–antivortex transformation with a particle–hole transformation:

$$b_i \to b_i^*, \tag{A11}$$
$$a_{ij} \to -a_{ij}, \tag{A12}$$
$$c_i \to \epsilon_i c_i^\dagger, \tag{A13}$$
$$f_i \to -\epsilon_i f_i^\dagger. \tag{A14}$$

Under this transformation $\hat{H}_2$ remains invariant. At the same time

$$\langle c_i^\dagger c_i\rangle \to 1 - \langle c_i^\dagger c_i\rangle. \tag{A15}$$

Theorem. In the presence of a KV The chemical potentials μ^c, and μ_i^f at half-filling is zero. Proof: In writing $\hat{H}_2$, μ^c, and μ_i^f is already set to be zero. We just need to prove that

$$\sum_{i\alpha} \langle c_{i\alpha}^\dagger c_{i\alpha}\rangle = \mathcal{N} \tag{A16}$$
$$\forall i : \sum_{\alpha} \langle f_{i\alpha}^\dagger f_{i\alpha}\rangle = 1. \tag{A17}$$

The proof is immediately obtained after combining lemma II and III, resulting in

$$\langle c_{i\alpha}^\dagger c_{i\alpha}\rangle = 1 - \langle c_{i\alpha}^\dagger c_{i\alpha}\rangle \Rightarrow \langle c_{i\alpha}^\dagger c_{i\alpha}\rangle = 1/2, \tag{A18}$$
$$\langle f_{i\alpha}^\dagger f_{i\alpha}\rangle = 1 - \langle f_{i\alpha}^\dagger f_{i\alpha}\rangle \Rightarrow \langle f_{i\alpha}^\dagger f_{i\alpha}\rangle = 1/2, \tag{A19}$$

where we have brought back the spin flavor index α. Summing over spin flavors and lattice sites result in Eqs. (A16) and (A17).

Appendix B: Analysis of the zero mode equations

In this appendix we analyze the zero mode equations in the continuum limit. To simplify notations we do this near $+\boldsymbol{k}_D$ node. We also drop the spin and node flavors for a cleaner notation. The quadratic Kondo Hamiltonian of Eq. (8) near $\boldsymbol{k}_D$ node is given by the following matrix

$$\mathcal{H} = \begin{pmatrix} v_c(q_1\tau_2 + q_2\tau_1) & b \\ b^* & -v_f\big[(q_1+a_1)\tau_2 + (q_2+a_2)\tau_1\big] \end{pmatrix}, \tag{B1}$$

where a_1, and a_2 are the spatial components of the gauge field. We study the zero energy solutions

$$\mathcal{H}\pi = 0 \tag{B2}$$

using the following gauge choice:

$$b(\boldsymbol{r}) = |b(r)|e^{i\theta}, \tag{B3}$$
$$\boldsymbol{a}(\boldsymbol{r}) = a_\theta(r)\hat{\boldsymbol{\theta}} = a_\theta(r)\left[-\sin\theta\hat{\boldsymbol{x}} + \cos\theta\hat{\boldsymbol{y}}\right]. \tag{B4}$$

π is given by

$$\pi = \begin{pmatrix} c_A \\ c_B \\ f_A \\ f_B \end{pmatrix}. \tag{B5}$$

Eq. (B2) is analyzed in real space by replacing $q_j = i\partial_j$. It also turns to be more elegant to switch from x and y to z and z^*:

$$z = x + iy \tag{B6}$$
$$z^* = x - iy \tag{B7}$$
$$2\partial_{z^*} = \partial_x + i\partial_y \tag{B8}$$
$$2\partial_z = \partial_x - i\partial_y \tag{B9}$$

Above equations lead to

$$(q_1+a_1)\tau_2+(q_2+a_2)\tau_1= \begin{pmatrix} 0 & 2\partial_{z^*}+e^{+i\theta}a(r) \\ -2\partial_z+e^{-i\theta}a(r) & 0 \end{pmatrix} \tag{B10}$$

By a trivial scaling we set $v_f=1$, and replace v_c with $\zeta=v_c/v_f$. A further scaling

$$\begin{pmatrix} c_A \\ c_B \end{pmatrix} \to \frac{1}{\sqrt{\zeta}} \begin{pmatrix} c_A \\ c_B \end{pmatrix}, \quad b \to \sqrt{\zeta} b \tag{B11}$$

eliminates ζ from the zero mode equations:

$$\begin{pmatrix} 0 & 2\partial_{z^*} & b & 0 \\ -2\partial_z & 0 & 0 & b \\ b^* & 0 & 0 & -2\partial_{z^*}-ae^{i\theta} \\ 0 & b^* & 2\partial_z-ae^{-i\theta} & 0 \end{pmatrix} \begin{pmatrix} c_A \\ c_B \\ f_A \\ f_B \end{pmatrix} = 0 \tag{B12}$$

The above equations are decoupled into two sets of (2-component) equations:

$$\begin{pmatrix} 2\partial_{z^*} & b & 0 & 0 \\ b^* & 2\partial_z-ae^{-i\theta} & 0 & 0 \\ 0 & 0 & -2\partial_z & b \\ 0 & 0 & b^* & -2\partial_{z^*}-ae^{i\theta} \end{pmatrix} \begin{pmatrix} c_B \\ f_A \\ c_A \\ f_B \end{pmatrix} = 0 \tag{B13}$$

If $a(r)=0$ only the upper-block leads to normalizeable solution[27]. The zero mode equations we are going to investigate are:

$$2\frac{\partial c_B}{\partial z^*}+bf_A=0 \tag{B14}$$

$$b^*c_B+(2\frac{\partial}{\partial z}-ae^{-i\theta})f_A=0 \tag{B15}$$

In polar coordinates $z=re^{i\theta}$

$$\frac{\partial}{\partial z}=\frac{e^{-i\theta}}{2}\frac{\partial}{\partial r}+\frac{e^{-i\theta}}{2ir}\frac{\partial}{\partial\theta} \tag{B16}$$

$$\frac{\partial}{\partial z^*}=\frac{e^{i\theta}}{2}\frac{\partial}{\partial r}-\frac{e^{i\theta}}{2ir}\frac{\partial}{\partial\theta}, \tag{B17}$$

and zero mode equations become:

$$e^{i\theta}\left(\frac{\partial}{\partial r}+\frac{i}{r}\frac{\partial}{\partial\theta}\right)c_B+b(\boldsymbol{r})f_A=0 \tag{B18}$$

$$b^*(\boldsymbol{r})c_B+e^{-i\theta}\left(\frac{\partial}{\partial r}-\frac{i}{r}\frac{\partial}{\partial\theta}-a_\theta(r)\right)f_A=0 \tag{B19}$$

As we know from the Ref. 27 the gauge flux does not change the number of zero modes, as gauge field can be scaled away in that case. There is also a topological proof using index theorem which shows the insensitivity of the zero modes to the gauge flux[28]. However in the Jackiw-Rossi case, the the gauge field is coupled to both fermions, i.e. $\left(\frac{\partial}{\partial r}+\frac{i}{r}\frac{\partial}{\partial\theta}\right)$ in Eq. (B18) is replaced with $\left(\frac{\partial}{\partial r}+\frac{i}{r}\frac{\partial}{\partial\theta}-a_\theta(r)\right)$. In contrast to the work of Jackiw and Rossi, the gauge field here can not be scaled away from the zero mode equations. This is because the gauge field is only coupled to f fermions.

We analyze the robustness of zero modes numerically where we fix κ_2 (charecterizing the phase twist in the b field) to be 1, and vary κ_1 (the ratio of the gauge flux to 2π) from 0 to 2. The numerical evidence (see Fig. 10 for an example) is a convincing evidence that gauge flux does not affect zero modes in our problem as well. We are able to show this analytically for 4π gauge flux. A proof for any gauge flux is desirable.

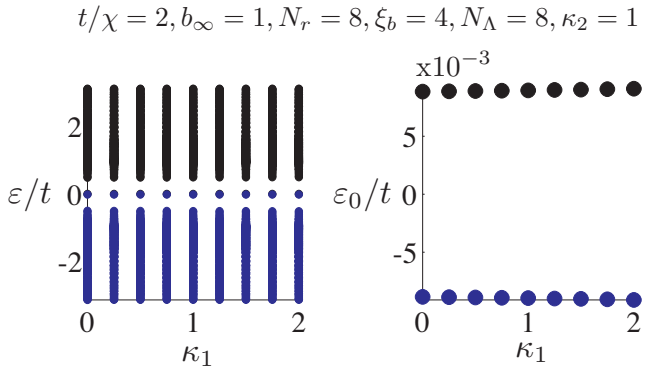

FIG. 10: The evolution of energy levels ε (in units of t), as a function of κ for one spin flavor. The left figure shows all the energies. The right shows only the two modes which are going to be *zero* modes in the infinite lattice limit. κ_1 is a fraction of 2π flux enclosed, and κ_2 characterizes the phase "twist" of the b field $b_i=|b_i|e^{i\kappa_2\theta_i}$. As can be seen from the right figure the variation of these "zero" modes compared to the 0 flux limit is marginal. It is a convincing numerical evidence that zero modes stay at zero for any gauge flux. We have an anlytical proof on the existence of 1 zero mode per node and per spin flavor for $\kappa_1=2$ point.

	$r\to 0$	$r\to\infty$
$\lvert b(r)\rvert$	$\propto r$	b_∞
$a_\theta(r)$	$\propto r$	$-1/r$

TABLE III: The asymptotic forms of a_θ and $|b|$. This information is the only thing we need to prove the existence of zero modes.

In the equations below we change $a_\theta\to 2a_\theta$ to discuss the 4π flux case. After replacing $b(\boldsymbol{r})=e^{i\theta}|b(r)|$ in above equations, the phase factors $e^{\pm i\theta}$ disappears from both sides. Therefore we seek solutions for c and f without any θ dependance:

$$\frac{\partial c_B}{\partial r}+|b|f_A=0 \tag{B20}$$

$$|b|c_B+\frac{\partial f_A}{\partial r}-2a_\theta f_A=0 \tag{B21}$$

These equations are regular as $r \to 0$. We need to find the solutions as $r \to \infty$,

$$\frac{\partial c_B}{\partial r} + b_\infty f_A = 0, \tag{B22}$$

$$b_\infty c_B + \frac{\partial f_A}{\partial r} + 2 f_A / r = 0, \tag{B23}$$

and show that a normalizeable branch exists.

The solutions for the above equations is given below:

$$c_B(r) = \frac{e^{-|b_\infty| r} I_1}{r} + \frac{e^{|b_\infty| r} I_2}{2|b_\infty| r}, \tag{B24}$$

$$f_A(r) = \frac{e^{-|b_\infty| r}}{b_\infty} \left(\frac{|b_\infty|}{r} + \frac{1}{r^2} \right) I_1 + \frac{e^{|b_\infty| r}}{2 b_\infty} \left(-\frac{1}{r} + \frac{1}{|b_\infty| r^2} \right) I_2. \tag{B25}$$

Therefore 1 exponentially decaying normalizable branch ($I_2 = 0$) exist, which proves the existence of 1 zero mode per spin per node flavor for the $\kappa_1 = 2$ case.

What we have proved here is that for a 4π gauge flux, (i.e. $a_\theta \to 2a_\theta$) one zero mode per spin and node flavor exists. We have also shown convincing numerical evidence that the existence of zero modes does not depend on the gauge flux, just like the classic Jackwi-Rossi case, albeit we can not prove this analytically in this case. Therefor we believe 1 zero mode per spin and node flavor exist for the 2π flux case, which is the case of interest.

[1] P. Coleman, and A. J. Schofield, Nature **433**, 226 (2005).
[2] H. v. Löhneysen *et al.*, Rev. Mod. Phys. **79**, 1015 (2007).
[3] H. v. Löhneysen et al., Phys. Rev. Lett. **72**, 3262 (1994).
[4] Mathur, N. D. et al., Nature **394**, 39-43 (1998).
[5] J. Custers et al., Nature **424**, 524 (2003).
[6] S. Paschen *et al.*, Nature **432**, 881 (2004).
[7] H. Shishido *et al.*, J. Phys. Soc. Jpn. **74**, 1103 (2005).
[8] S. Doniach, Physica B **91**, 231 (1977).
[9] T. Senthil, S. Sachdev, and M. Vojta, Phys. Rev. Lett. **90**, 216403 (2003); T. Senthil, M. Vojta, and S. Sachdev, Phys. Rev. B **69**, 035111 (2004).
[10] P. G. Niklowitz , G. Knebel, J. Flouquet, S. L. Bud'ko, and P. C. Canfield, Phys. Rev. B 73, 125101 (2006).
[11] Nakatsuji, S. et al. Nature Phys. 4, 603607 (2008).
[12] Friedemann, S. et al. Nature Phys. 5, 465469 (2009)
[13] J. Hertz, Phys. Rev. B **14**, 1165 (1976); T. Moriya, *Spin Fluctuations in Itinerant Electron Magnetism*, Springer-Verlag, Berlin (1985); A. J. Millis, Phys. Rev. B **48**, 7183 (1993).
[14] P. Coleman, arXiv:cond-mat/0206003v3.
[15] I. Affleck, and J. B. Marston, Phys. Rev. B **37**, 3774 (1988); J. B. Marston, and I. Affleck, Phys. Rev. B **39**, 11538 (1989).
[16] S. Saremi, P. A. Lee, and T. Senthil, arXiv:0903.4195.
[17] G. 't Hooft, F. Bruckmann, arXiv:hep-th/0010225v1.
[18] S. Coleman, *Aspects of Symmetry* (Cambridge University Press, Cambridge, UK, 1985).
[19] T. Senthil *et al.*, Science **303**, 1490 (2004); T. Senthil *et al.*, Phys. Rev. B **70**, 144407 (2004).
[20] S. Saremi, and P. A. Lee, Phys. Rev. B **75**, 165110 (2007).
[21] T. Senthil, S. Sachdev, and M. Vojta, Physica B 359-361, 9 (2005).
[22] M. Hermele *et al.*, Phys. Rev. B **77**, 224413 (2008).
[23] J. Alicea *et al.*, Phys. Rev. B **72**, 064407 (2005).
[24] J. Alicea, O. I. Motrunich, and M. P. A. Fisher, Phys. Rev. B **73**, 174430 (2006).
[25] M. P. A. Fisher, and D. H. Lee, Phys. Rev. B **39**, 2756 (1989).
[26] N. Nagaosa, and P. A. Lee, Phys. Rev. B **61**, 9166 (2000).
[27] R. Jackiw, and P. Rossi, Nuclear Physics B **190**, 681 (1981).
[28] E. Weinberg, Phys. Rev. D **24**, 2669 (1981).